ELSEVIER

Ceramics International 31 (2005) 737–742

CERAMICS INTERNATIONAL

www.elsevier.com/locate/ceramint

Electrical and microstructural properties of (Zn, Nb, Fe)-doped SnO_2 varistor systems

R. Parra[a,*], J.A. Varela[b], C.M. Aldao[a], M.S. Castro[a]

[a]*Institute of Materials Science and Technology (INTEMA, CONICET-UNMdP), J.B. Justo 4302, B7608FDQ Mar del Plata, Argentina*
[b]*Instituto de Química, UNESP, P.O. Box 355, 14801-970 Araraquara, SP, Brazil*

Received 30 April 2004; received in revised form 14 June 2004; accepted 13 August 2004
Available online 9 December 2004

Abstract

The electrical and microstructural properties of SnO_2-based varistors with the addition of 0.025 and 0.050 mol% of Fe_2O_3 have been characterised. Electric field (E) versus current density (J) curves showed that the effect of Fe_2O_3 addition is to increase both the non-linear coefficient and the breakdown voltage. Variations in the potential barrier height were inferred from impedance spectroscopy (IS) analysis. Through transmission electron microscopy (TEM), the presence of precipitates of secondary phases was confirmed. Samples with precipitates displayed poor electrical properties.

Keywords: B. Microstructure-final; C. Electrical properties; C. Impedance; E. Varistors; Tin dioxide

1. Introduction

Metal oxide varistors are electronic ceramic devices whose function is to sense and limit transient voltage surges and to do so repeatedly without being destroyed or damaged [1,2]. Their non-linear current–voltage behaviour is described by the equation $I = V^{\alpha}$, where α is the non-linearity coefficient whose magnitude is strongly influenced by the addition of transition metal oxides to the varistor composition [3,4].

Tin dioxide is an n-type wide band gap semiconductor with a very low densification rate due to its high surface diffusion at low temperatures and high SnO_2 partial vapour pressure at sintering temperatures [5]. Pianaro et al. reported that doping with CoO and Nb_2O_5 drastically improve the sinterability of SnO_2 [6]. Wang et al. achieved high density values of SnO_2 doped with ZnO and Nb_2O_5 [7]. The role of the oxygen vacancies generated by these transition metal oxides as the driving force for densification has been thoroughly treated in the literature [8–10].

The attractive feature of SnO_2-based varistors is their fairly simple microstructure that reveals single phase systems under X-ray powder diffraction (XRD) resolution. However, precipitated phases occurring at grain boundaries and triple points have been recently found through the transmission electron microscopy (TEM) technique in SnO_2-based systems containing La_2O_3, Pr_2O_3 and Fe_2O_3 [11–13]. The effect of such secondary phases on the electrical properties of the devices is not completely clear and calls for special attention.

Antunes et al. attained improvements in the non-linear behaviour of the SnO_2–CoO–Nb_2O_5 system by the addition of small amounts of Fe_2O_3 [14]. They associated the modified behaviour to the creation of point defects due to the solid solution of Fe_2O_3 into the host lattice. On the other hand, devices with an acceptable non-linear coefficient have also been obtained doping SnO_2 with ZnO and Nb_2O_5 [7,15].

The purpose of the present work is to analyse the influence of Fe_2O_3 on the electrical properties and on the microstructure of the ternary system SnO_2–ZnO–Nb_2O_5. The effect of inhomogeneities in the microstructure is also addressed.

* Corresponding author.
E-mail address: rparra@fi.mdp.edu.ar (R. Parra).

0272-8842/$30.00
doi:10.1016/j.ceramint.2004.08.009

2. Experimental procedure

Analytical grades of SnO_2 (Aldrich), ZnO (Baker), Nb_2O_5 (Fluka AG), and Fe_2O_3 (Baker) were mixed in an alcoholic medium in order to obtain homogeneous compositions as listed in Table 1. The resulting slurries were dried at 65 °C for 48 h and subsequently sieved through a 43 μm mesh screen. Powders were pressed without any binder into discs by uniaxial pressing (80 MPa) followed by isostatic pressing (200 MPa). Finally, the pellets were sintered in air at 1300 °C for 2 h with heating and cooling rates of 3 °C/min in an RHF 17/6S Carbolite furnace.

The apparent density of sintered samples was estimated by the Archimedes method. X-ray powder diffraction analyses were carried out with a Rigaku 22000 equipment running with Cu Kα radiation. Refinements through the Rietveld method yielded values of the lattice parameters.

Microstructural characterisation of polished specimens was performed by scanning electron microscopy (SEM), in a Philips 505 microscope, and by transmission electron microscopy, in a Philips CM200 instrument operating at 200 kV.

Mean grain sizes were estimated over SEM micrographs through the method of the intercept proposed by Mendelson [16].

Selected area diffraction (SAD) patterns were obtained in order to identify the different phases present in the microstructures. The fundamental relationship in a diffraction pattern,

$$Rd = \lambda L \quad (1)$$

where R is any distance measured on the pattern related to a specific d spacing in the crystal and λL is the microscope constant, was applied. The TEM was equipped with an EDS (PGT PRISM-digital spectrometer) system for energy dispersive X-ray analysis.

Sintered samples were lapped to ensure plane parallel faces where silver electrodes were deposited for electrical characterisation. A Keithley 237 high voltage source-measure unit was used to acquire plots of the current density J as a function of the electric field E. The electrical breakdown field E_r was measured at 1 mA cm^{-2} current density and the nonlinear coefficient α was estimated from room temperature J–E curves by equation (2),

$$\alpha = \frac{1}{\log\left(E_{10\,\mathrm{mA}}/E_{1\,\mathrm{mA}}\right)} \quad (2)$$

where $E_{10\ \mathrm{mA}}$ and $E_{1\ \mathrm{mA}}$ are the electric fields corresponding to current densities of 10 and 1 mA cm^{-2}, respectively [3]. Impedance spectroscopy (IS) measurements were carried out by means of an HP 4194A impedance analyser with an amplitude voltage of 0.5 V in the frequency range of 100 Hz–15 MHz and in the temperature range of 30–200 °C. Plots of the imaginary ($-Z''$) versus the real (Z') component of impedance were fitted with a simple R(RC) electrical model. Grain and grain boundary resistances were determined from the intercepts of the fitted semicircles with the Z' axis at the high and low frequency regions, respectively. The capacitance was obtained from the maximum value of Z''.

3. Results and discussion

Although no other phases besides that of rutile were revealed in the XRD patterns of the sintered samples, the lattice parameters suffered small changes with the addition of Fe_2O_3 in comparison to the starting SZN powder as recorded in Table 2. These changes are within the order of magnitude of those reported in the literature for systems with the addition of 0.050% Fe_2O_3 [14]. A diminution in the unit cell volume could be caused by Fe^{3+} species of smaller ionic radius (0.64 Å) than that of Sn^{4+} (0.71 Å) in agreement with former results [11,14]. Interestingly, no further cell contraction was observed after increasing the amount of Fe_2O_3 to 0.050 mol%, fact attributed to the low solubility of iron into the host lattice.

SEM micrographs of sintered samples in Fig. 1 show homogeneous microstructures with mean grain sizes around 3 μm; relative densities and mean grain sizes are listed in Table 3. Densities above 96% of the SnO_2 theoretical density were achieved with the incorporation of ZnO and Nb_2O_5 to SnO_2, and a further densification was attained with the addition of Fe_2O_3. It has been proved that the oxygen vacancies created by the Sn^{4+} substitution by Zn^{2+}, Co^{2+}, Co^{3+}, Fe^{3+}, Mn^{2+} and Mn^{3+} among other ions, enhance the material densification through the activation of diffusion and material transport mechanisms [8–10]. These mechanisms did enhance the densification of the samples under study, but a noticeable grain growth did not take place with the addition of iron oxide.

Precipitated secondary phases containing Sn, Zn and Fe were found in the SZN–0.050% Fe_2O_3 microstructure through EDS-assisted TEM. The grains and their composition are indicated in Fig. 2. The selected area diffraction patterns allowed the identification of the tin oxide phase and led to the awareness of the multiphase nature of the secondary phases. The presence of the Zn_2SnO_4 cubic phase

Table 1
Sample composition (mol%)

Sample	SnO_2	ZnO	Nb_2O_5	Fe_2O_3
SZN	98.975	1.0	0.025	–
SZN–0.025% Fe_2O_3	98.950	1.0	0.025	0.025
SZN–0.050% Fe_2O_3	98.925	1.0	0.025	0.050

Table 2
Lattice parameters of the sintered samples

Sample	a (Å)	c (Å)	V (Å^3)
SZN	4.7355(7)	3.1850(6)	71.4235
SZN–0.025% Fe_2O_3	4.7345(7)	3.1845(7)	71.3821
SZN–0.050% Fe_2O_3	4.7343(7)	3.1843(7)	71.3716

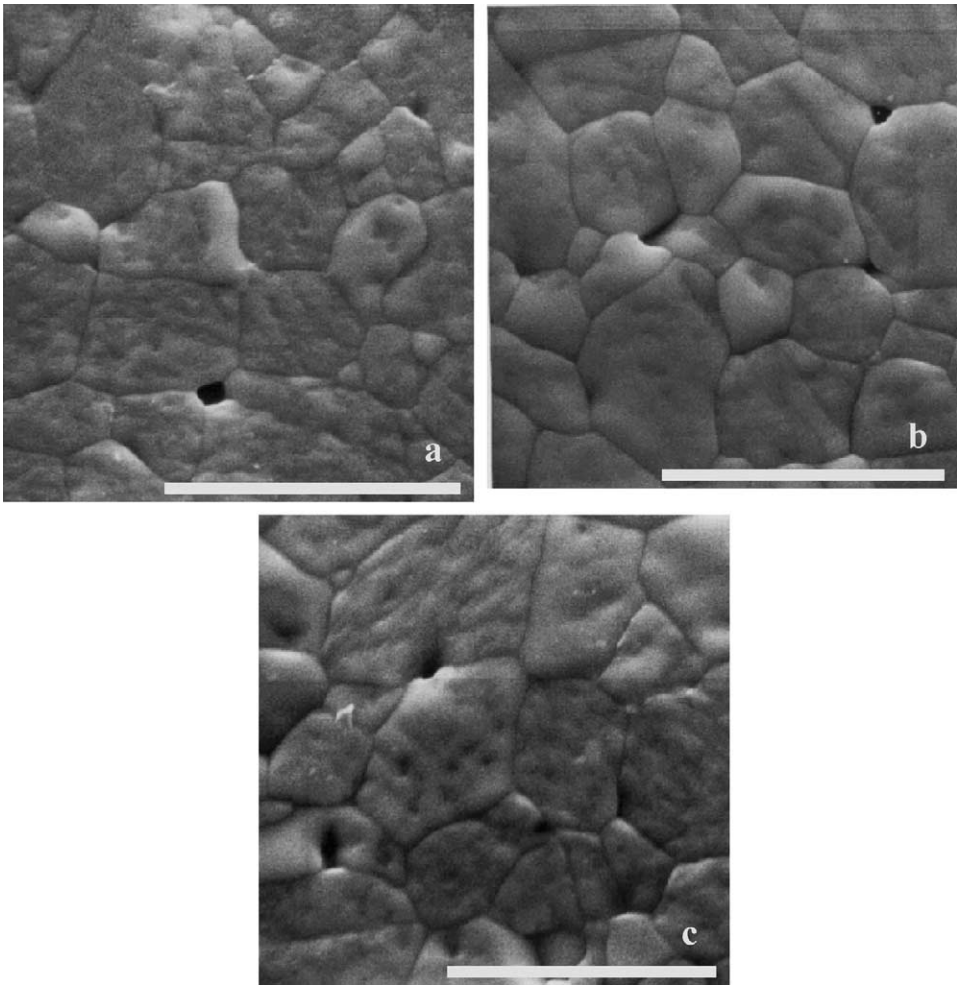

Fig. 1. SEM micrographs of polished samples sintered at 1300 °C for 2 h: (a) SZN; (b) SZN–0.025% Fe_2O_3; and (c) SZN–0.050% Fe_2O_3. Bar = 10 μm.

in the precipitates composition was inferred from the study of the SAD patterns and the JCP-DS 73-1725 file.

In Fig. 3 we present the room temperature *J*–*E* curves for the different specimens studied. Sample SZN displayed the lowest resistivity and a poor non-linearity, whereas samples SZN–0.025% Fe_2O_3 and SZN–0.050% Fe_2O_3 exhibited improved non-linear properties. In Table 3, the main parameters that characterise the varistor behaviour, the electric breakdown field E_r and the non-linear coefficient α, are listed. From these findings, it was determined that the addition of iron (III) oxide to the SZN–varistor composition improves the non-ohmic features and increases the breakdown field. Similar conclusions are found in the literature for the typical compositions of devices based on SnO_2–Co_3O_4–Nb_2O_5 [11] and SnO_2–CoO–Nb_2O_5 [14], showing a similar effect of Fe^{3+} over all of these systems. As well as other transition metal oxides such as Bi_2O_3, La_2O_3 and Cr_2O_3, Fe_2O_3 segregates at grain boundaries where it induces changes in the concentration of the atomic defects at grain–grain interfaces. On the other hand, the arise of phases that concentrate the additives have a negative effect on the electrical properties. These phases hinder the homogeneous distribution of metal oxides along boundary regions and preclude them from trapping negatively charged species, which are responsible for the Schottky-type barrier characteristics. Therefore, the diminution, though slight, in the α value for the SZN–0.050% Fe_2O_3 system suggests that the existence of secondary phases might modify the electronic states of the grain boundary region. Similar results were found for the SnO_2–CoO–Ta_2O_5–La_2O_3 system [13].

Table 3
Relative density (ρ_r), mean grain size, breakdown electric field (E_r) and non-linearity coefficient (α) for samples sintered at 1300 °C for 2 h

Sample	ρ_r (%)	d (μm)	E_r (V/cm)	α
SZN	96.6	3.7	1300	7
SZN–0.025% Fe_2O_3	96.9	3.9	2290	11
SZN–0.050% Fe_2O_3	97.8	3.9	2430	9

SnO_2 theoretical density = 6.95 g cm^{-3}.

Complementary electrical characterisation was accomplished by means of IS. Experimental data recorded at several temperatures are represented in Fig. 4 as plots of the imaginary versus the real component of impedance. Table 4 shows the outcomes derived from the 80 °C curves. From the

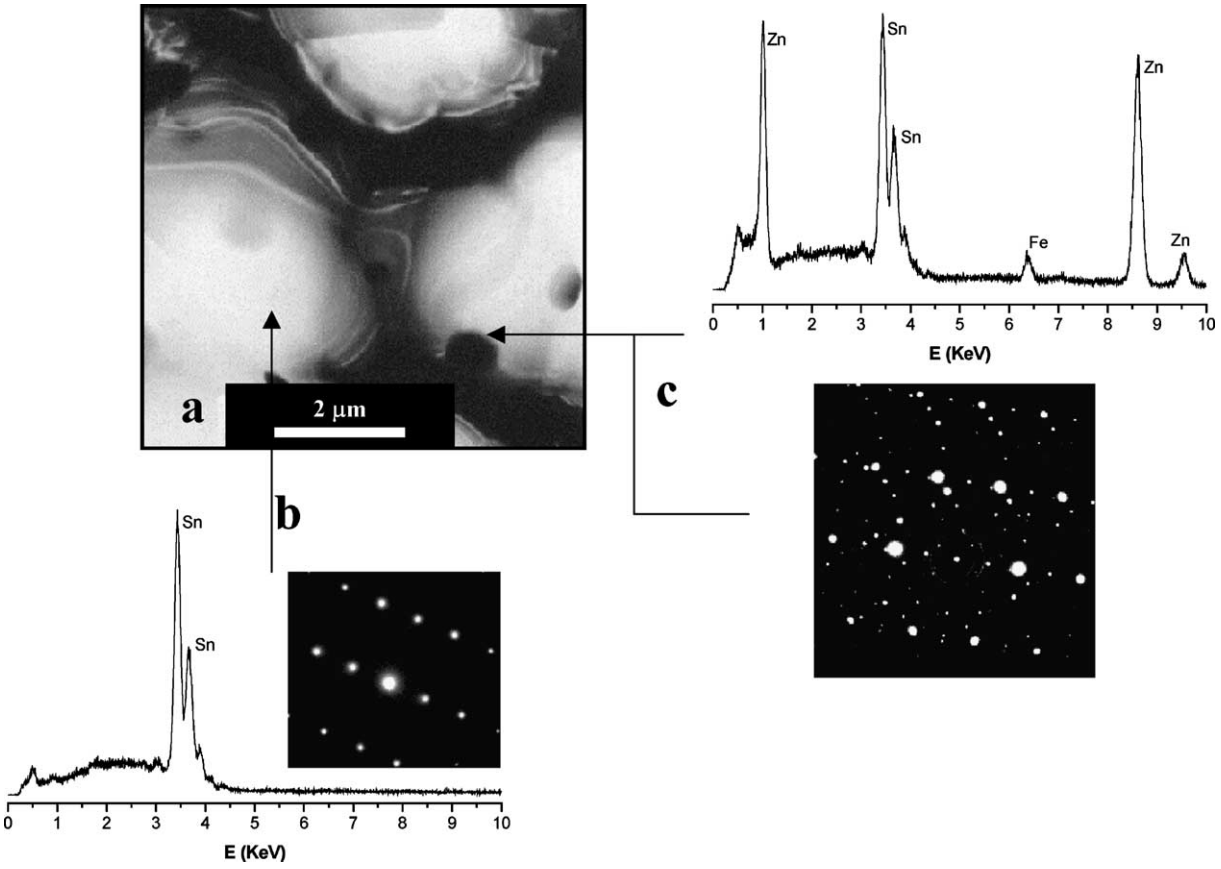

Fig. 2. (a) TEM image of SZN–0.050% Fe_2O_3 sample; (b) EDS analysis and SAD pattern of grain region; and (c) EDS analysis and SAD pattern of the precipitates.

capacitance values, the grain boundary is determined to dominate the samples impedance in agreement with previous studies [17]. Further, information was obtained from the temperature dependence of the total resistance. The electric conduction can be described as a thermally activated process, then

$$\ln\left(\frac{1}{R}\right) = \ln A_0 - \frac{E_a}{kT}, \tag{3}$$

where R is the grain resistance (R_g) plus the grain boundary resistance (R_{gb}), A_0 is the pre-exponential factor, E_a is the effective activation energy for carrier migration, k is the Boltzmann constant and T the absolute temperature [18]. Effective activation energies for conduction were obtained from the slopes of the $\ln(1/R)$ versus $1/T$ Arrhenius-type plots in Fig. 5; the results are shown in Table 4. The values for R_g and R_{gb} show that the response of the device is controlled by the grain boundary. Leite et al. assigned the occurrence of distinct activation energies to the response of different defects in the low and high temperature ranges of

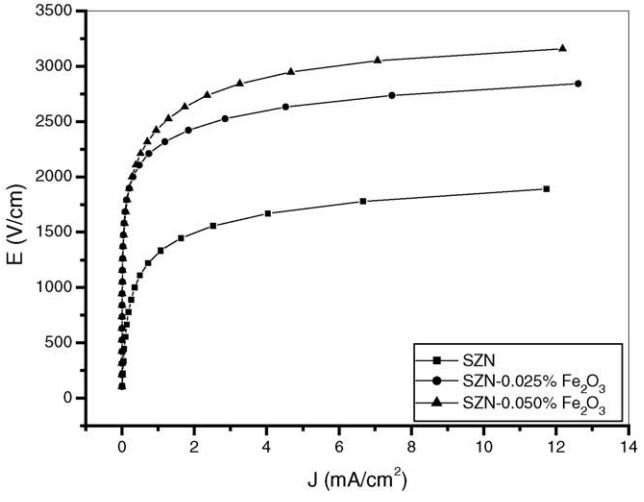

Fig. 3. *J–E* characteristic curves on a linear scale of sintered samples at room temperature.

Table 4
Grain boundary resistance (R_{gb}), grain resistance (R_g) and capacitance at 80 °C and effective activation energy for conduction (E_a)

Sample	R_{gb} (Ω)	R_g (Ω)	C (F)	E_a (eV)
SZN	1.3×10^5	1.2	5.2×10^{-10}	0.18
SZN–0.025% Fe_2O_3	4.5×10^5	2	1.7×10^{-10}	0.19
SZN–0.050% Fe_2O_3	3.5×10^6	13	1.3×10^{-10}	0.24

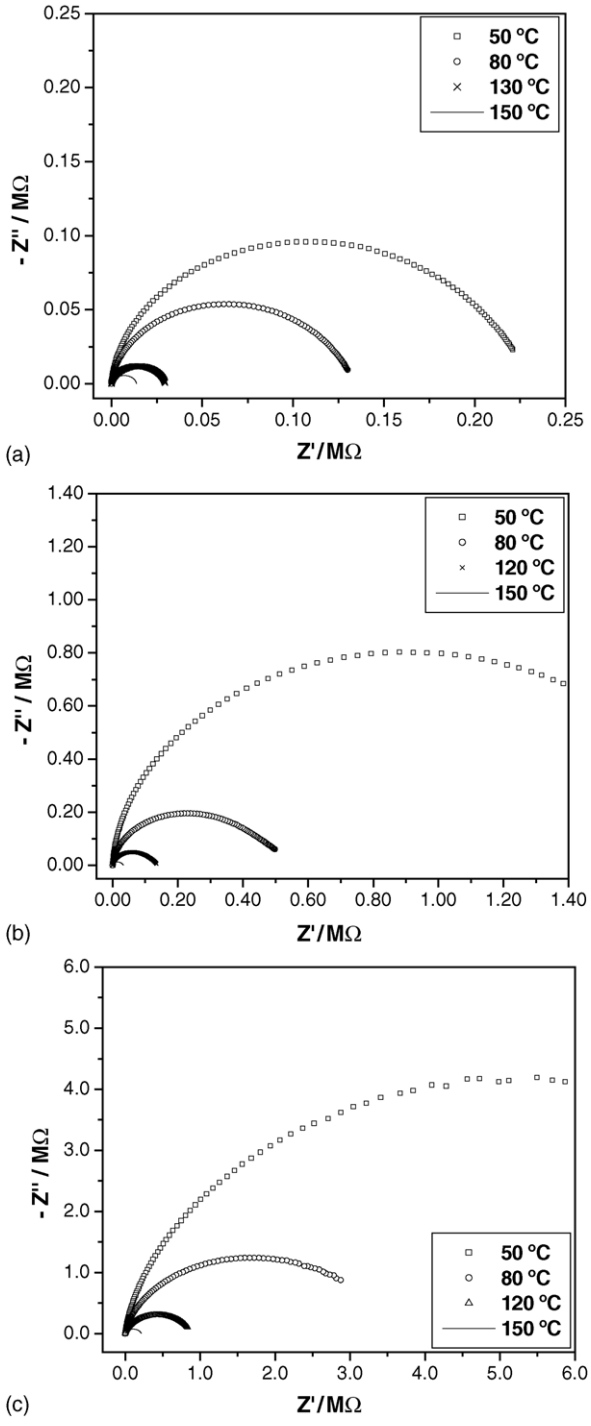

Fig. 4. Cole–cole plots at different temperatures for sintered samples (a) SZN, (b) SZN–0.025% Fe_2O_3, and (c) SZN–0.050% Fe_2O_3.

50–200 °C and 200–400 °C, respectively [19]. Within the temperature range selected for the impedance measurements, it is not possible to distinguish discrete regions corresponding to different activation energies. When the Fe_2O_3 mol% is increased from 0.025 to 0.050, the E_a is significantly raised; observation that would account for the arising of atomic defects electrically active at grain boundaries that heightens the potential barrier.

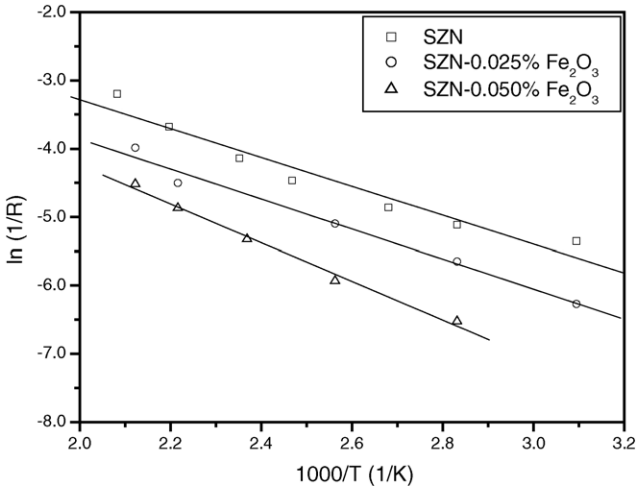

Fig. 5. ln(1/R) vs. 1/T plots for the samples under characterisation.

In a Schottky-type barrier, the capacitance is related to the electron concentration in the bulk, n, and to the barrier height, ϕ_B, as

$$C \propto \left(\frac{n}{\phi_B}\right)^{1/2} \quad (4)$$

A diminution in the capacitance could then be ascribed to an increase in the potential barrier height, to a decrease in the donor concentration or eventually, to both phenomena occurring simultaneously. Sample SZN displayed the highest capacitance; this is consistent with the high donor concentration normally expected for this sample. The lowest potential barrier is also inferred from the results in Table 4. The capacitance shows a small variation between the Fe_2O_3-doped samples; however, the R_{gb} value at 80 °C of the SZN–0.050% Fe_2O_3 sample is an order of magnitude higher than that of the SZN–0.025% Fe_2O_3, phenomenon associated to changes in the boundary characteristics. More than one semicircle could show up in a cole–cole plot due to the presence of secondary phases; but plots in Fig. 4 show simple curves with only one semicircle in each particular case. However, some of the arcs are not absolutely symmetric suggesting that small semicircles at the low frequency side of the plots could be present. An increase in the bulk resistance is also observed with the addition of iron oxide as shown in Table 4. This lower grain conductivity might be associated to a lower degree in the Nb^{5+}/Sn^{4+} substitution as Fe^{3+} more likely substitutes Sn^{4+} due to its smaller ionic radius with respect to that of Nb^{5+}.

4. Conclusions

The following conclusions are derived from the experimental results here reported.

1. Addition of Fe_2O_3 improved the non-linear properties of the (Zn, Nb)-doped SnO_2 varistor. Its segregation to grain

boundaries contributes to increase the potential barrier height.

2. Secondary phases containing Sn, Zn and Fe were observed through EDS-assisted TEM. Samples with secondary phases showed poorer non-linear properties.
3. The effective activation energy E_a for conduction as well as the potential barrier height is raised when Fe_2O_3 is incorporated to the varistor composition since it contributes to the barrier formation at the grain–grain interface. Grain resistance is also affected by Fe_2O_3 addition due to the competitive effect between Nb^{5+} and Fe^{3+} for a place in the lattice.

Acknowledgements

The authors are grateful to the Programa CYTED (Proyecto PI-VIII.13 PROALERTA), to CONICET and ANPCyT (Argentina), to CNPq and FAPESP (Brazil) for the financial support provided for this research.

References

[1] L.M. Levinson, H.R. Philipp, Zinc-oxide varistors: a review, Am. Ceram. Soc. Bull. 65 (1998) 639–646.
[2] M. Matsuoka, Progress in research and development of zinc oxide varistors, in: L.M. Levinson (Ed.), Grain Boundary Phenomena in Electronic Ceramics, vol. 1, Advances in Ceramics, The American Ceramic Society Inc., Ohio, 1981, pp. 290–308.
[3] T.K. Gupta, Application of zinc oxide varistors, J. Am. Ceram. Soc. 73 (1990) 1817–1840.
[4] S.A. Pianaro, P.R. Bueno, E. Longo, J.A. Varela, Microstructure and electric properties of a SnO_2-based varistor, Ceram. Int. 25 (1991) 1–6.
[5] S.A. Pianaro, P.R. Bueno, P. Olivi, E. Longo, J.A. Varela, Effect of Bi_2O_3 on the microstructure and electrical properties of the SnO_2–CoO–Nb_2O_5 varistor system, J. Mater. Sci. Lett. 16 (1997) 634–638.
[6] S.A. Pianaro, P.R. Bueno, E. Longo, J.A. Varela, A new SnO_2-based varistor system, J. Mater. Sci. Lett. 14 (1995) 692–694.
[7] Y. Wang, J. Wang, H. Chen, W. Zhong, P. Zhang, H. Dong, L. Zhao, Electrical properties of SnO_2–ZnO–Nb_2O_5 varistor system, J. Phys. D: Appl. Phys. 33 (1996) 96–99.
[8] M.S. Castro, C.M. Aldao, Characterization of SnO_2-varistors with different additives, J. Eur. Ceram. Soc. 18 (1998) 2233–2239.
[9] F. Fayat, M.S. Castro, Defect profile and microstructural development in SnO_2-based varistors, J. Eur. Ceram. Soc. 23 (2003) 1585–1591.
[10] J.A. Varela, L.A. Perazolli, E. Longo, E.R. Leite, J.A. Cerri, Effect of atmosphere and dopants on sintering of SnO_2, Radiat. Eff. Defects Solids 146 (1996) 131–143.
[11] R. Parra, M.S. Castro, J.A. Varela, Analysis of secondary phases segregated and precipitated in SnO2-based varistors, J. Eur. Ceram. Soc. 25 (2005) 401–406.
[12] M.M. Oliveira, P.C. Soares Jr., P.R. Bueno, E.R. Leite, E. Longo, J.A. Varela, Grain-boundary segregation and precipitates in La_2O_3 and Pr_2O_3 doped SnO_2.CoO-based varistors, J. Eur. Ceram. Soc. 23 (2003) 1875–1880.
[13] L.G.P. Simões, P.R. Bueno, M.O. Orlandi, E.R. Leite, E. Longo, The influence of excess precipitate on the non-ohmic properties of SnO_2-based varistors, J. Electroceram. 10 (2003) 63–68.
[14] A.C. Antunes, S.R.M. Antunes, A.J. Zara, S.A. Pianaro, E. Longo, J.A. Varela, Effect of Fe_2O_3 doping on the electrical properties of a SnO_2-based varistor, J. Mater. Sci. 37 (2002) 2407–2411.
[15] J.F. Wang, Y.J. Wang, W.B. Su, H.C. Chen, W.X. Wang, Novel (Zn, Nb)-doped SnO_2 varistors, Mater. Sci. Eng. B (2002) 8–13.
[16] M.I. Mendelson, Average grain size in polycrystalline ceramics, J. Am. Ceram. Soc. 52 (1969) 443.
[17] D.C. Sinclair, F.D. Morrison, A.R. West, Applications of combined impedance and electric modulus spectroscopy to characterise electroceramics, Int. Ceram. 2 (2002) 33–37.
[18] Z. Branković, G. Branković, D. Poleti, J.A. Varela, Structural and electrical properties of ZnO varistors containing different spinel phases, Ceram. Int. 27 (2001) 115–122.
[19] E.R. Leite, A.M. Nascimento, P.R. Bueno, E. Longo, J.A. Varela, The influence of sintering process and atmosphere on the non-ohmic properties of SnO_2-based varistor, J. Mater. Sci.: Mater. Electron. 10 (1999) 321–327.